nature neuroscience

Dopaminergic and glutamatergic microdomains in a subset of rodent mesoaccumbens axons

Shiliang Zhang[1], Jia Qi[1], Xueping Li[1,4], Hui-Ling Wang[1], Jonathan P Britt[2,4], Alexander F Hoffman[3], Antonello Bonci[2], Carl R Lupica[3] & Marisela Morales[1]

Mesoaccumbens fibers are thought to co-release dopamine and glutamate. However, the mechanism is unclear, and co-release by mesoaccumbens fibers has not been documented. Using electron microcopy, we found that some mesoaccumbens fibers have vesicular transporters for dopamine (VMAT2) in axon segments that are continuous with axon terminals that lack VMAT2, but contain vesicular glutamate transporters type 2 (VGluT2). *In vivo* overexpression of VMAT2 did not change the segregation of the two vesicular types, suggesting the existence of highly regulated mechanisms for maintaining this segregation. The mesoaccumbens axon terminals containing VGluT2 vesicles make asymmetric synapses, commonly associated with excitatory signaling. Using optogenetics, we found that dopamine and glutamate were released from the same mesoaccumbens fibers. These findings reveal a complex type of signaling by mesoaccumbens fibers in which dopamine and glutamate can be released from the same axons, but are not normally released at the same site or from the same synaptic vesicles.

The simple notion of a dopamine pathway projecting from ventral tegmental area (VTA) to nucleus accumbens (nAcc) has been complicated by several recent findings. Neurons that project from the VTA to nAcc are molecularly diverse, and may release dopamine, glutamate or GABA. In addition, activation of nAcc fibers from neurons expressing the dopamine transporter (DAT) causes glutamate release in nAcc[1,2]. It has been suggested that VTA dopamine neurons co-release dopamine and glutamate, but anatomical evidence shows that nAcc axons identified by tyrosine hydroxylase immunoreactivity (TH-IR) make only symmetric synapses in nAcc and do not express any of the known vesicular glutamate transporters[3–5]. Thus, the structural basis for the proposed co-release of dopamine and glutamate in the nAcc is unclear.

Two sub-classes of VTA neurons expressing *Vglut2* (also known as *Slc17a6*) mRNA target the rat nAcc[6,7]. The cell bodies of one of them express *Vglut2* mRNA without detectable levels of TH-IR (VGluT2-only neurons), whereas the other sub-class of neurons coexpress *Vglut2* mRNA and TH (VGluT2-TH neurons). It is unclear what type of synapses these neurons establish in the nAcc. The detection of *Vglut2* mRNA and TH protein in VTA cell bodies[7,8] is consistent with earlier *in vitro* electrophysiological studies demonstrating glutamatergic neurotransmission by mesencephalic TH-IR primary cultures, and the hypothesis that dopamine neurons co-release dopamine and glutamate[9,10]. Optogenetic studies have further demonstrated that the VGluT2-TH mesoaccumbens neurons appear to use glutamate as a signaling molecule[1,2], although whether VGluT2-TH neurons release dopamine in brain tissue remains to be demonstrated.

Although recent phenotypic analysis of rat VTA has shown that VGluT2-TH neurons contain aromatic acid decarboxylase[11], and are therefore capable of synthesizing dopamine, it is unclear whether these neurons have the capacity to co-release dopamine and glutamate from the same or different subcellular neuronal structures. Although some findings provide evidence for a lack of vesicular colocalization of dopamine and glutamate, others support the idea of vesicular coexistence of dopamine and glutamate. For instance, findings from high-resolution imaging of intact brain tissue indicate that TH and VGluT2 are not coexpressed in the same terminals in the nAcc of adult rats[4,5] or in mice of any age[3]. However, other studies have reported vesicular co-immunoprecipitation of VMAT2 and VGluT2 in nAcc preparations, leading to the hypothesis that, in the nAcc, vesicular glutamate co-entry has a synergistic effect on vesicular dopamine filling and that glutamate and dopamine are co-released in the nAcc from the same pool of vesicles[12,13].

To determine whether dopamine and glutamate share the same axon terminals (ATs) or vesicles, we examined the ultrastructural, biochemical and electrophysiological properties of VGluT2 inputs from VTA neurons in the nAcc. We found that the dual VGluT2-TH neurons from both rat and mouse have separate ultrastructural domains for the accumulation and release of either dopamine or glutamate. Specifically, VGluT2 from VGluT2-TH neurons was present in synaptic vesicles of ATs forming asymmetric synapses, whereas VMAT2-IR or TH-IR was present in only a subset of these neurons. Moreover, VMAT2 and TH-IR were present in adjacent segments that did not overlap with the terminals containing VGluT2 vesicles, and *in vivo* overexpression of VMAT2 did not disrupt the segregation between VGluT2 and VMAT2. Although nAcc vesicles did not coexpress VGluT2 and VMAT2, optogenetic activation of

[1]National Institute on Drug Abuse, Neuronal Networks Section, US National Institutes of Health, Baltimore, Maryland, USA. [2]National Institute on Drug Abuse, Synaptic Plasticity Section, US National Institutes of Health, Baltimore, Maryland, USA. [3]National Institute on Drug Abuse, Electrophysiology Research Section, US National Institutes of Health, Baltimore, Maryland, USA. [4]Present address: Xi'an Medical University, Xi'an, China (X.L.), and Department of Psychology, McGill University, Montreal, Quebec, Canada (J.P.B.). Correspondence should be addressed to M.M. (mmorales@intra.nida.nih.gov).

Received 2 December 2014; accepted 13 January 2015; published online 9 February 2015; doi:10.1038/nn.3945

nAcc fibers from VTA VGluT2-TH neurons evoked AMPA/NMDA receptor–mediated excitatory postsynaptic currents (EPSCs) and the release of dopamine. We conclude that both VGluT2-only and VGluT2-TH neurons form mesoaccumbens glutamatergic pathways that parallel the well-known mesoaccumbens dopaminergic pathway, and that VGluT2-TH neurons in the rat and mouse possess two distinct contiguous domains that are specialized for either dopamine or glutamate release.

RESULTS

Rat mesoaccumbens ATs containing VGluT2 establish asymmetric synapses; those containing TH establish symmetric synapses

We previously showed that two types of putative glutamatergic VTA neurons (VGluT2-only and VGluT2-TH neurons) innervate the nAcc[7]. Here we sought to determine the type of synapses that these VTA neurons establish in the shell of the nAcc. We tagged axons from the rat VTA by intra-VTA injections of the anterograde tract tracer *Phaseolus vulgaris* leucoagglutinin (PHA-L) or an adeno-associated virus (AAV) encoding mCherry under the control of the *Camk2a* promoter (**Fig. 1a**). With both tracers, we found that some ATs from VTA neurons in the nAcc containing VGluT2 immunoreactivity (VGluT2-IR) formed asymmetric synapses on the heads of dendritic spines or dendritic shafts (**Fig. 1b**). We determined that 96.09 ± 2.70% of the PHA-L$^+$ ATs that established asymmetric synapses also expressed VGluT2 (70 of 72 ATs, $n = 3$ rats, $t_2 = 17.07$, $P = 0.0034$; **Fig. 1b**). Among the few ATs with TH-IR that formed synapses, most of those expressing PHA-L formed symmetric synapses (95.24 ± 4.76%, 17 of 18 ATs, $n = 3$ rats, $t_2 = 9.50$, $P = 0.0109$; **Fig. 1c**). The infrequent detection of TH$^+$ terminals making synapses has been previously documented[14]. We also observed VGluT2$^+$ terminals and TH$^+$ terminals that lacked PHA-L, indicating that not all mesoaccumbens cells were tagged and, in the case of VGluT2 terminals, indicating that some of these terminals do not originate from the VTA. In addition, we found ultrastructural arrangements in which an mCherry-labeled terminal (from a VTA VGluT2 neuron) formed an asymmetric synapse on the head of a dendritic spine that also received a symmetric convergent mCherry input (from a VTA TH neuron) on the neck of the spine (**Fig. 1d–f**).

Subcellular segregation of dopaminergic and glutamatergic signaling by rat VTA neurons

We next explored the possibility that segregation between dopaminergic and glutamatergic signaling may occur in the same axon. We first determined the distribution of TH-IR and VGluT2-IR in serial sections of nAcc from wild-type rats immunolabeled before ultrathin sectioning (pre-embedding immunolabeling). In this procedure, the antigen-antibody complexes were identified by silver-intensified gold or peroxidase reaction. We occasionally observed TH$^+$ axon segments contiguous with VGluT2$^+$ ATs (**Fig. 2a** and **Supplementary Fig. 1**). In some instances, a TH$^+$ axon segment making a symmetric synapse (in this domain) was contiguous with a VGluT2$^+$ AT; in this case, the AT established an asymmetric synapse with a dendritic spine (**Supplementary Fig. 1**). From these findings, we conclude that, under normal conditions, axons from rat VGluT2-TH neurons maintain independent, but adjacent, cellular compartments in the nAcc containing either TH or VGluT2 protein, but not both.

As with TH detection, DAT was frequently observed in the nAcc. We occasionally detected DAT signal confined to an axon segment continuous with a VGluT2-IR terminal making an asymmetric synapse on the head of a dendritic spine (**Fig. 2b**). To further characterize the properties of the axon segments adjacent to VGluT2$^+$ terminals derived from rat VGluT2-TH neurons, we determined the specificity of several antibodies to VMAT2. Of eight tested antibodies, one showed selectivity for VMAT2 detection (EB06558 antibody; **Supplementary Fig. 2**), which we used to determine the distribution of VMAT2-IR in relation to VGluT2-IR. Although we observed numerous VMAT2- or VGluT2-labeled terminals in the nAcc, we did not find double-labeled ATs that would indicate colocalization of VMAT2 and VGluT2. However, we occasionally observed examples of VMAT2-IR in the axon segment proximal to a VGluT2$^+$

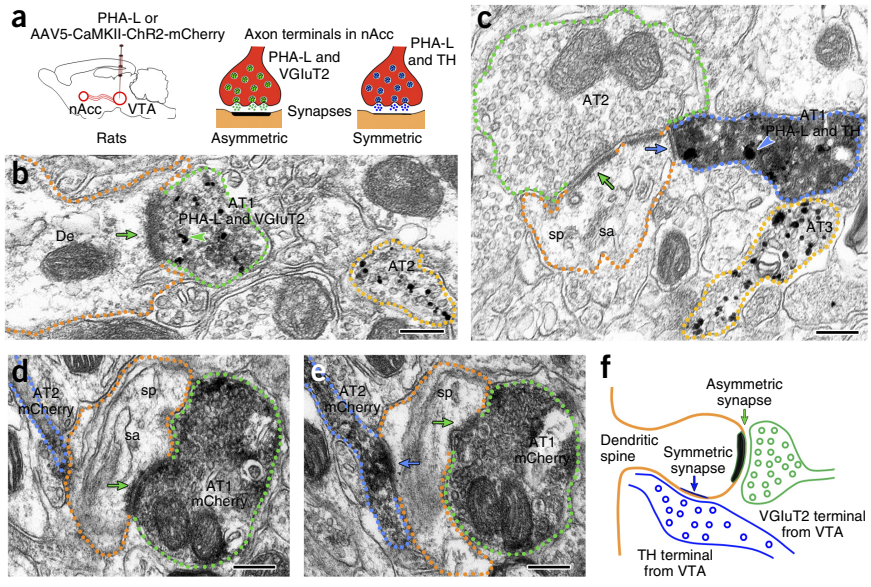

Figure 1 Mesoaccumbens neurons establish either VGluT2-asymmetric synapses or TH-symmetric synapses (wild-type rats). (**a**) VTA inputs to nAcc identified by PHA-L or mCherry immunoreactivity. VTA neurons were tagged with PHA-L ($n = 3$ rats) or AAV5-CaMKII-ChR2-mCherry ($n = 2$ rats). In the nAcc, PHA-L-IR ATs made asymmetric or symmetric synapses onto dendrites or dendritic spines. (**b**) nAcc AT1 (AT1, green outline) coexpressing PHA-L (scattered dark material) and VGluT2 (gold particles, green arrowhead) made an asymmetric synapse (green arrow) with a dendrite (De, orange outline). AT2 (yellow outline) contained only VGluT2. (**c**) nAcc AT1 (blue outline) coexpressing PHA-L (scattered dark material) and TH (gold particles, blue arrowhead) made a symmetric synapse (blue arrow) on the side of a dendritic spine (sp, orange outline) with spine apparatus (sa). The head of this dendritic spine also made an asymmetric synapse (green arrow) with the unlabeled AT2 (green outline). AT3 (yellow outline) showed only TH-IR. (**d**–**f**) Triad arrangement in which ATs from VTA neurons converged on the same dendritic spine and established different types of synapses. Shown are serial sections of two ATs from VTA neurons expressing mCherry (scattered dark material) under the control of the *Camk2a* promoter (**d**,**e**). Both ATs made synapses on the same dendritic spine (sp, orange outline); AT1 (green outline) made an asymmetric synapse (green arrow) on the head of the spine and AT2 (blue outline) made a symmetric synapse (blue arrow) on the side of the same dendritic spine. Scale bars represent 200 nm (**b**–**e**).

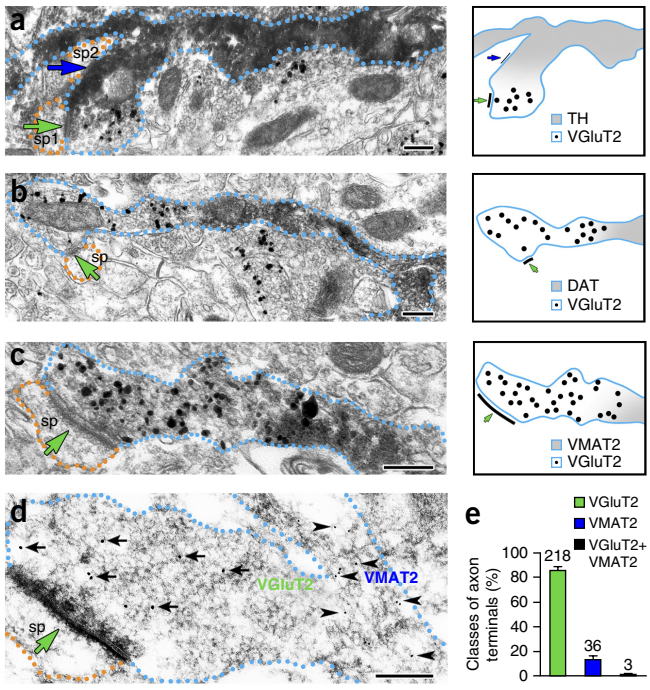

Figure 2 Mesoaccumbens axons from VGluT2-TH neurons segregate dopaminergic markers and VGluT2 to different micro-domains (wild-type rats). (**a**–**c**) Pre-embedding detection of VGluT2-IR in ATs lacking dopaminergic markers, which establish asymmetric synapses (green arrows) on dendritic spines (orange outlines). VGluT2-IR (gold particles) was confined to the ATs. The contiguous axon segments to these VGluT2 terminals contained TH-IR (scattered dark material in **a**), DAT-IR (scattered dark material in **b**) or VMAT2-IR (scattered dark material in **c**). Note that the axon containing TH-IR established a symmetric synapse (blue arrow in **a**). ATs were quantified from the nAcc of rats ($n = 4$). (**d**) Post-embedding detection of VGluT2-IR (18-nm gold particles, black arrows) in an AT lacking VMAT2-IR and establishing an asymmetric synapse (green arrow) on a dendritic spine (orange outline). The contiguous axon segment to this VGluT2$^+$ terminal contained VMAT2-IR (12-nm gold particles, black arrowheads). (**e**) Bars indicating the frequency (mean + s.e.m.) of ATs containing VGluT2-IR or VMAT2-IR from a total of 257 ATs. Of these ATs, 85.48 ± 3.03% expressed VGluT2, 13.37 ± 2.78% expressed VMAT2 and 1.15 ± 0.40% appeared to coexpress VGluT2 and VMAT2 (paired t test, $t_3 = 12.42$, $P = 0.0011$). ATs were quantified from the nAcc of rats ($n = 4$). Scale bars represent 200 nm (**a**–**d**).

terminal making an asymmetric synapse on the head of a dendritic spine (**Fig. 2c**). Because pre-embedding immunolabeling may result in the differential penetration of antibodies, we further evaluated the pattern of VGluT2 and VMAT2 distribution using a 'post-embedding' double immunolabeling procedure. In this procedure, ultrathin sections of the nAcc shell were probed with antibodies to VGluT2 or VMAT2 and detected with secondary antibodies bound to colloidal gold of two different sizes. Consistent with results from pre-embedding labeling, post-embedding labeling revealed that, when present in the same axon, VMAT2-IR was in the axon segment proximal to a VGluT2$^+$ terminal making an asymmetric synapse on the head of a dendritic spine (**Fig. 2d**). We determined that 85.48 ± 3.03% of the labeled ATs expressed VGluT2, 13.37 ± 2.78% expressed VMAT2, and 1.15 ± 0.40% appeared to coexpress VGluT2 and VMAT2 (**Fig. 2e**). From these findings, we suggest that VGluT2-TH neurons can store glutamate (via VGluT2) and dopamine (via VMAT2) in distinct vesicular populations that are differentially segregated in subcellular compartments in the same axon.

Our ultrastructural findings provide evidence that the storage of dopamine and glutamate in the nAcc takes place in distinct vesicular pools enriched in different axonal micro-domains. However, to determine whether our ultrastructural techniques lacked the sensitivity for co-detection of VGluT2 and VMAT2, we next explored the possibility of coexistence of VGluT2 and VMAT2 at the vesicular level by immunolabeling and by co-immunoprecipitation of VGluT2 and VMAT2 from vesicles obtained from rat nAcc synaptomes. After testing several conditions of isolation for synaptic vesicles, we achieved experimental conditions (Online Methods) that allowed the purification of a homogeneous population of synaptic vesicles, the quality and purity of which were confirmed by electron microscopy analysis (**Fig. 3a**).

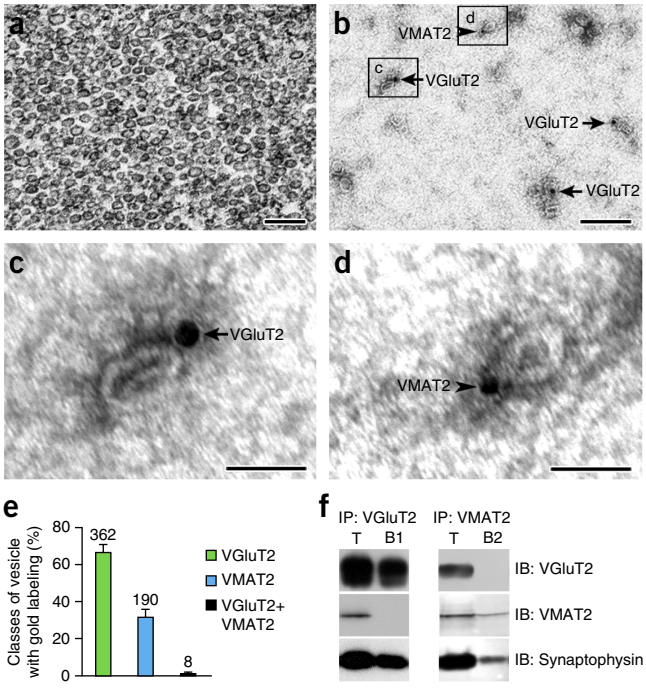

Figure 3 VGluT2 and VMAT2 localize to distinct subpopulations of synaptic vesicles (wild-type rats). (**a**) Electron micrograph showing the purity and integrity of nAcc-isolated synaptic vesicles used for either dual detection of VGluT2-IR and VMAT2-IR (**b**–**d**) or co-immunoprecipitation of VGluT2 and VMAT2 (**f**). (**b**–**d**) Detection of VGluT2-IR (arrows, 18-nm gold particles) or VMAT2-IR (arrowheads, 12-nm gold particles) associated with purified synaptic vesicles. (**e**) Bars indicating the frequency (mean + s.e.m.) of vesicles containing VGluT2-IR or VMAT2-IR from a total of 560 labeled vesicles. Of these vesicles, 66.74 ± 4.10% expressed VGluT2, 31.71 ± 3.99% expressed VMAT2 and 1.55 ± 0.35% appeared to colabel for VGluT2 and VMAT2 (paired t test, $t_2 = 4.333$, $P = 0.0493$). Synaptic vesicles were quantified from three different preparations of isolated vesicles from the nAcc of rats ($n = 110$). (**f**) Western blots of proteins from isolated vesicles before immunoprecipitation (IP, T) and after IP with antibodies against VGluT2 (IP: VGluT2, B1) or VMAT2 (IP: VMAT2, B2). Western blots were immunolabeled (IB) with antibodies to VGluT2, VMAT2 or the vesicular marker synaptophysin. The vesicular nature of each fraction was confirmed by the detection of synaptophysin. VGluT2 and VMAT2 were present in the total pool of vesicles (T). In contrast, VGluT2 was detected only in the sample IP with antibody to VGluT2 (IP: VGluT2), and VMAT2 was detected only in the sample IP with antibody to VMAT2. The western blots were successfully repeated at least three times. Full-length blots are presented in **Supplementary Figure 3**. Scale bars represent 200 nm (**a**,**b**) and 50 nm (**c**,**d**).

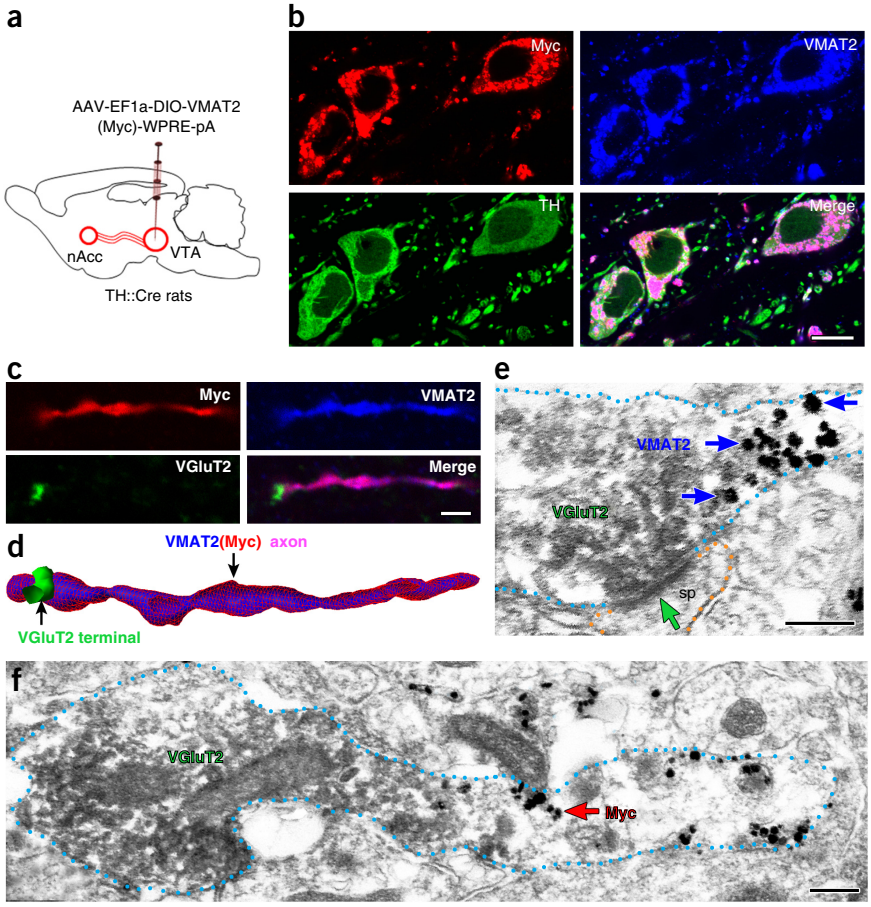

Figure 4 Subcellular segregation of VGluT2-IR and VMAT2(Myc)-IR in the same VGluT2-TH axon from a *Th-Cre* rat overexpressing VMAT2(Myc) under the regulation of the *Th* promoter (TH-VMAT2(Myc) rats). (**a**) Schematic representation of VTA inputs (identified by Myc and VMAT2 content) to nAcc. VGluT2-TH and TH-only neurons were infected by injections of AAV-EF1a-DIO-VMAT2(Myc)-WPRE-pA into the VTA of *Th-Cre* rats (TH-VMAT2(Myc) rats, $n = 4$). (**b**) Immunofluorescence detection of Myc-IR (red), VMAT2-IR (blue) and TH-IR (green) in the medial VTA. Myc-IR, VMAT2-IR and TH-IR were detected in the same cell bodies and processes. (**c**,**d**) Immunofluorescence detection of Myc-IR (red), VMAT2-IR (blue) and VGluT2-IR (green) in the nAcc. (**c**) Myc-IR and VMAT2-IR were present in the same axon, but VGluT2-IR was restricted to a terminal-like structure lacking both Myc-IR and VMAT2-IR. (**d**) The VGluT2$^+$ terminal-like structure in continuum to an axon coexpressing Myc and VMAT2 is better seen in this three-dimensional reconstruction from *z* stack confocal microscopy images. (**e**,**f**) Electron micrographs of ATs containing VGluT2-IR (scattered dark material), but lacking both VMAT2-IR and Myc-IR (gold particles). The VGluT2$^+$ AT is adjacent to an axon segment that contains VMAT2-IR (blue arrow, gold particles in **e**) or Myc-IR (red arrows, gold particles in **f**). Note in **e** that the AT containing VGluT2-IR established an asymmetric synapse (green arrow). Scale bars represent 10 µm (**b**), 2 µm (**c**) and 200 nm (**e**,**f**).

By immunolabeling these isolated synaptic vesicles, we detected two distinct pools of vesicles, those containing VGluT2 and those containing VMAT2 (**Fig. 3b–d**). We found that, of 560 labeled vesicles, 66.74 ± 4.10% expressed VGluT2, 31.71 ± 3.99% expressed VMAT2, and a very small proportions (1.55 ± 0.35%) appeared to colabel for VGluT2 and VMAT2 (**Fig. 3e**). The lack of coexistence of VGluT2 and VMAT2 at the vesicular level was next confirmed by co-immunoprecipitation of VGluT2 and VMAT2 from the isolated vesicles. Consistent with our ultrastructural findings, protein preparations of vesicles immunoprecipitated with antibodies to VGluT2 showed vesicular immunodetection of both VGluT2 and the vesicular marker synaptophysin, but not VMAT2 (**Fig. 3f** and **Supplementary Fig. 3a**). Moreover, protein preparations of vesicles immunoprecipitated with antibodies to VMAT2 showed vesicular immunodetection of both VMAT2 and synaptophysin, but not VGluT2 (**Fig. 3f** and **Supplementary Fig. 3a**). Thus, we conclude that accumulation of dopamine by VMAT2 occurs in vesicles different from those that accumulate glutamate by VGluT2 (**Supplementary Fig. 3b**).

To further validate the detection of subcellular segregation between VGluT2 and VMAT2 in mesoaccumbens axons, we selectively induced *in vivo* overexpression of VMAT2 with the Myc tag at the amino terminus (VMAT2(Myc)) in dopamine neurons by injecting an AAV vector encoding Cre-inducible VMAT2(Myc) in the VTA of *Th-Cre* rats (**Fig. 4a**). By triple immunofluorescence (TH-VMAT2(Myc)), we confirmed Myc expression confined to VTA-TH neurons coexpressing VMAT2 (**Fig. 4b**). In the nAcc, we observed axons with dual VMAT2(Myc) immunolabel contiguous with VGluT2$^+$ terminals (**Fig. 4c**,**d**). By three-dimensional analysis, we found that the vast majority of mesoaccumbens VGluT2 terminals lacked VMAT2(Myc) (99.45 ± 0.08%, 8,548 of 8,593 ATs) ($t_3 = 527.00$, $P = 0.0001$). In addition, we confirmed by electron microscopy the ultrastructural presence of VGluT2 in ATs (making asymmetric synapses) that were adjacent to axon segments containing VMAT2 (**Fig. 4e**) or Myc (**Fig. 4f**). We determined that the majority of ATs expressing VGluT2 lacked VMAT2 or Myc (98.84 ± 0.64%, 160 of 162 ATs, $t_3 = 75.94$, $P = 0.0002$). These findings suggest that VMAT2(Myc) overexpression in mesoaccumbens axons from VGluT2-TH neurons does not alter the segregation between VGluT2 and VMAT2.

As in the rat, VGluT2-only and VGluT2-TH neurons establish asymmetric VGluT2-terminals in the mouse nAcc

Recent findings indicate that a subset of neurons coexpressing TH-mRNA and VGluT2-mRNA lack detectable levels of TH-protein in their cell bodies and axons[15]. Thus to determine whether the mouse VGluT2-TH neurons innervating the nAcc, as those in the rat, segregate TH-IR and VGluT2-IR in the same axons, we injected an AAV vector encoding Cre-inducible light-activated channelrhodopsin2 (ChR2) tethered to mCherry into the VTA of *Th-Cre* and *Vglut2-Cre* mice (**Fig. 5a** and **Supplementary Figs. 4a** and **5a**). In the VTA of infected *Th-Cre* mice (TH-ChR2-mCherry mice, $n = 3$), we detected mCherry only in neurons expressing *Th* mRNA (**Supplementary Fig. 4b–e**). Of 576 mCherry$^+$ neurons, 97.85 ± 0.83% coexpressed *Th* mRNA (**Supplementary Fig. 4f**), indicating that mCherry was selectively expressed by the *Th* promoter. In addition, we detected coexpression of mCherry and TH in neurons located in the VTA (**Fig. 5b**), corresponding to the location of dopamine neurons innervating the nAcc[16]. Because VGluT2 protein is undetectable in cell bodies of glutamatergic neurons, we determined the selectivity of mCherry

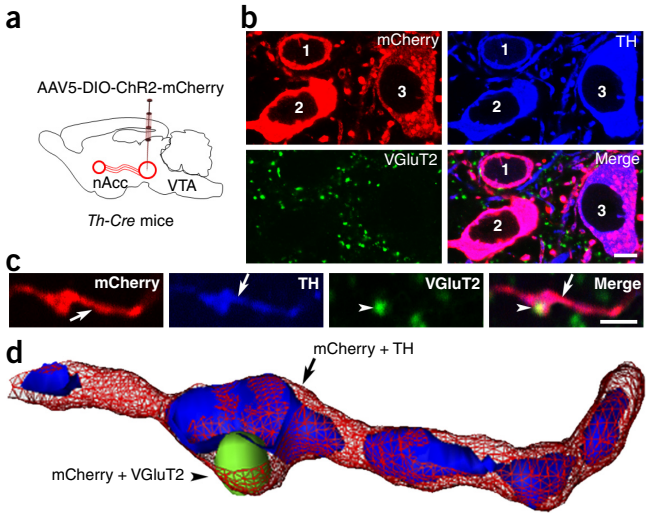

Figure 5 VGluT2-TH neurons segregate VGluT2 and TH to distinct subcellular compartments in the same axon (*Th-Cre* mice). (**a**) Schematic representation of nAcc inputs from VTA neurons expressing mCherry under the control of the *Th* promoter (TH-ChR2-mCherry mice, $n = 4$). (**b**–**d**) Fluorescence detection of mCherry-IR (red), TH-IR (blue) and VGluT2-IR (green) in the lateral VTA and nAcc. (**b**) In the VTA, mCherry-IR was detected in cell bodies (1, 2 and 3) and processes. These mCherry$^+$ cell bodies lacked VGluT2-IR, but TH-IR was present. In the nAcc, mCherry (under the control of the *Th* promoter) was detected throughout the axon (red in **c**). In contrast, VGluT2-IR was restricted to a terminal-like structure (arrowheads in **c**). TH-IR was present in segments in the mCherry$^+$ axon (arrows in **c**). (**d**) Segregation among one VGluT2 terminal-like structure and TH axon segments in the same nAcc axon from a VGluT2-TH neuron is better seen in this three-dimensional reconstruction from *z* stack confocal microscopy images of triple labeled nAcc. Scale bars represent 5 µm (**b**) and 2 µm (**c**).

expression under the *Vglut2* promoter via detection of Vglut2 mRNA in mCherry-expressing neurons taken from VTA tissue by laser-capture dissection. Using real-time quantitative reverse transcription PCR (qRT-PCR) analysis of individual micro-dissected neurons, we confirmed the selective expression of mCherry under the *Vglut2* promoter (**Supplementary Fig. 5b**,**c**). We found that the ultrastructural features of TH or VGluT2 mesoaccumbens synapses from mice expressing mCherry under the *Th* promoter (TH-ChR2-mCherry; **Supplementary Fig. 6a**) or under the *Vglut2* promoter (VGluT2-ChR2-mCherry) were indistinguishable; the mCherry terminals making asymmetric synapses contained VGluT2 protein, but not TH protein (**Supplementary Fig. 6b**), and those making symmetric synapses contained TH protein, but not VGluT2 protein (**Supplementary Fig. 6c**). These ultrastructural findings provide evidence that, as in the rat, the VGluT2-TH neurons make TH terminals, which are distinct from their VGluT2 terminals, and that their postsynaptic targets on dendritic spines are mutually exclusive (**Supplementary Fig. 6d**). We observed examples in which a single VGluT2 terminal (from TH-ChR2-mCherry mice or VGluT2-ChR2-mCherry mice) established multiple synapses in the nAcc (**Supplementary Fig. 6e**–**g**), indicating that a single VGluT2 terminal can affect multiple postsynaptic neurons.

As in the rat, there is subcellular segregation of dopaminergic and glutamatergic signaling by mouse VTA neurons

To determine whether the axonal compartmentalization between VGluT2-IR and TH-IR observed in the rat nAcc was also present in the mouse, we examined by triple immunofluorescence microscopy the cellular distribution of TH-IR and VGluT2-IR with respect to mCherry-IR in the nAcc of TH-ChR2-mCherry mice (**Fig. 5c**,**d**). In the nAcc of these mice, we observed VGluT2 terminal–like structures in single mCherry axons (**Fig. 5c**). By three-dimensional reconstruction, we found cases of TH$^+$ and VGluT2$^+$ microdomains along some mCherry axons, without apparent subcellular overlapping between TH-IR and VGluT2-IR (**Fig. 5d**). We observed a high frequency of mCherry-VGluT2–labeled varicosities that lacked TH-IR (94.63 ± 0.63%, 1,507 of 1,584 varicosities, $t_3 = 81.65$, $P = 0.0001$). Thus, we conclude that the mouse axons from VGluT2-TH neurons, as in rats, maintain cellular compartmentalization between TH protein and VGluT2 protein in the same axons in the nAcc. In addition to dual VGluT2-TH axons, we observed TH$^+$ axons in the nAcc of TH-ChR2-mCherry mice that did not express VGluT2 (**Supplementary Fig. 7a**–**e**). Under two-dimensional view, TH-IR appeared to be present in segments in mCherry$^+$ axons and ATs (**Supplementary Fig. 7b**). However, the distribution of TH-IR throughout the axon and ATs was better seen after three-dimensional reconstruction (**Supplementary Fig. 7c**). The presence of TH-IR throughout the mCherry$^+$ axon was confirmed by electron microscopy of serial sections (**Supplementary Fig. 7d**,**e**). These findings indicate that axonal micro-domains lacking TH-IR are characteristic of VGluT2-TH neurons, but not of TH-only neurons.

To determine whether the genetic manipulation of the *Th* gene in *Th-Cre* mice caused alterations in intra-axonal segregation between TH and VGluT2 signals, we used *Vglut2-Cre* mice to drive expression of mCherry under the *Vglut2* promoter. As detailed above, mCherry expression under the *Vglut2* promoter was found in both VGluT2-only and VGluT2-TH neurons (**Supplementary Fig. 5d**,**e**). As in the case of findings from *Th-Cre* mice, some axons expressing mCherry under the *Vglut2* promoter expressed TH. However, TH-IR was excluded from those terminal-like structures containing VGluT2-IR (**Supplementary Fig. 5f**,**g**). Thus, quantitative immunofluorescent findings from both *Th-Cre* and *Vglut2-Cre* driver lines, together with our ultrastructural findings from analysis of nAcc in the wild-type rat, provide convergent evidence that VGluT2-TH neurons synthesize both TH protein and VGluT2 protein and segregate them into different micro-domains in the same axon.

nAcc photo-stimulation of VGluT2 afferents from VTA neurons elicits EPSCs and dopamine release

Our ultrastructural findings demonstrating that VGluT2-ATs from both VGluT2-only and VGluT2-TH neurons establish asymmetric terminals in the nAcc suggest that these VGluT2 terminals use glutamate as a signaling molecule. To evaluate glutamatergic signaling by VGluT2 mesoaccumbens terminals, we stimulated VGluT2-ChR2-mCherry fibers using 473-nm light pulses delivered into nAcc slices (**Fig. 6a**–**c**). As previously reported, using whole-cell recordings of NAcc medium spiny neurons, we found that local photo-stimulation of VGluT2-ChR2-mCherry fibers evoked EPSCs (47 ± 14 pA, $n = 16$ neurons from 3 mice) that depended on both AMPA and NMDA receptors (AMPA/NMDA ratio 1.9 ± 0.4, $n = 5$ neurons from 3 mice)[13]. As detailed above, there is electrophysiological evidence indicating that some VTA-TH neurons can release glutamate in the nAcc[1,2]. However, it remains to be determined whether some of the same neurons also release dopamine. We applied fast-scan cyclic voltammetry to evaluate dopamine release by VGluT2-TH neurons following photo-stimulation of VGluT2-ChR2-eYFP fibers in nAcc slices. We found that selective photo-stimulation of fibers from VTA VGluT2-expressing neurons evoked nAcc phasic release of dopamine (**Fig. 6d**–**j**), which was elevated in response to incremental numbers of light pulses

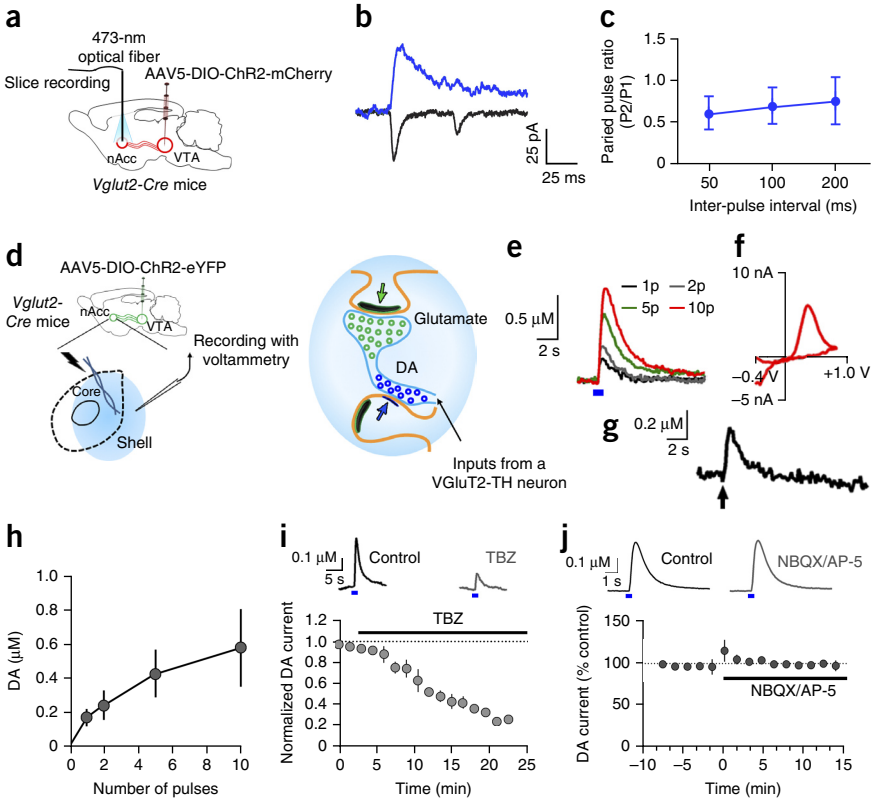

Figure 6 Photo-stimulation of mesoaccumbens VGluT2 fibers expressing ChR2 under the control of the *Vglut2* promoter elicits EPSCs and dopamine release in nAcc (*Vglut2-Cre* mice). (**a**–**c**) Photo-stimulation of nAcc fibers from VGluT2 VTA neurons ($n = 6$ VGluT2-ChR2-mCherry mice). (**b**) Optically evoked EPSCs recorded in nAcc shell. (**c**) Paired pulse ratios (P2/P1) in nAcc neurons (mean ± s.e.m., $n = 9$ per time point). (**d**) Electrically or optically evoked dopamine (DA) were measured by voltammetry. (**e**) Optically evoked dopamine release was increased in response to the increment of the number of pulses; 5-ms pulses (blue box) at 25 Hz. (**f**) Dopamine voltammogram in response to ten pulses of photo-stimulation. (**g**) Electrically evoked dopamine release (10 × 1-ms pulses at 25 Hz, arrow) at the same location of photo-stimulation. (**h**) Summary of dopamine release in response to the number of optical pulses (mean ± s.e.m., $n = 6$ slices from 3 mice). (**i**) Bath application of the VMAT2 inhibitor tetrabenazine (TBZ, 10 µM) significantly reduced optically evoked dopamine release (mean ± s.e.m., $P = 0.02$ versus control, paired t test, $n = 4$ slices from 2 mice). (**j**) Optically evoked dopamine responses from VGluT2-TH neurons were not dependent on glutamate receptors. Traces show optically evoked (25 Hz, 5 pulses, 5 ms) nAcc voltammetric currents measured before and after application of the glutamate receptor antagonists NBQX (5 µM) and AP-5 (40 µM). Graph shows the time course summary (mean ± s.e.m., $n = 4$ recordings from 2 mice); NBQX and AP-5 were applied during the time indicated by the bar. No significant effect on the dopamine signals was observed (two-tailed paired t test, $t_3 = 0.1239$, $P = 0.9093$).

(**Fig. 6h**) and was significantly reduced by bath application of the VMAT2 inhibitor tetrabenazine ($P = 0.02$ versus control; **Fig. 6i**). To determine whether light-evoked dopamine responses from VGluT2-TH neurons were dependent on glutamate receptors, we measured dopamine release in the nAcc before and following application of the glutamate receptor antagonists NBQX (5 µM) and AP-5 (40 µM). These antagonists did not significantly alter the light-evoked dopamine signals ($P = 0.9093$; **Fig. 6j**). These findings indicate that dopamine is synthesized, stored via a VMAT2-dependent process, and released directly by mesoaccumbens fibers arising from VGluT2-TH neurons.

DISCUSSION

By using anatomical, biochemical and electrophysiological approaches, we demonstrate that the VGluT2-TH neurons from the VTA of rats or mice have distinct ultrastructural domains for the accumulation and release of either dopamine or glutamate. The axon terminals from VTA VGluT2-TH neurons form two distinct types of synapses within the nAcc: asymmetric synapses by their VGluT2-axon terminals and symmetric synapses by their TH-axon terminals. We found that these two distinct types of axon terminals may derived from a single axon, as VMAT2-IR and TH-IR are present in axon segments adjacent to axon terminals containing VGluT2. Consistent with these anatomical findings, selective activation of mesoaccumbens terminals from VGluT2-TH neurons evoke both monosynaptic glutamate receptor-mediated currents in nAcc neurons and local release of dopamine. Thus VGluT2-TH neurons in the rat and the mouse possess two distinct contiguous domains that are specialized for either dopamine or glutamate release.

The presence in the nAcc of a triad arrangement between dopaminergic and glutamatergic inputs from amygdala, hippocampus or cortex on the same postsynaptic structure is well established[17], and been proposed as a synaptic arrangement by which midbrain dopamine release modulates excitatory transmission at the level of individual dendritic spines[18]. Here, we provide evidence of convergence of inputs from VGluT2-mesoaccumbens neurons and TH-mesoaccumbens neurons on a single postsynaptic target. We do not know whether the VGluT2 terminals in a triad arrangement are from VGluT2-only or VGluT2-TH neurons, as the mesoaccumbens VGluT2 terminals from both type of neurons share the same ultrastructural features. Because we previously found that some VTA VGluT2-TH neurons, but not VGluT2-only neurons, have D2 receptors[11], we suggest that if glutamatergic axon terminals from VGluT2-TH neurons containing dopamine D2 receptors participate in the formation of triad arrangements, their glutamate release would be regulated by neighboring dopamine. In this regard, electrophysiological studies have shown that EPSCs mediated by activation of mesoaccumbens fibers are inhibited by the dopamine D2 receptor antagonist sulpiride[19].

By applying two sensitive methods of immunodetection at the ultrastructural level ("pre-embedding" and "post-embedding" immunolabeling), we found that both rat and mouse mesoaccumbens axons from VGluT2-TH neurons have distinct microdomains for either glutamate or dopamine signaling. We suggest that VGluT2-TH neurons can store glutamate (via VGluT2) and dopamine (via VMAT2) in distinct vesicular populations that are differentially segregated in subcellular compartments in the same axon, as we found that single mesoaccumbens axons have VMAT2-IR within an axon segment proximal to a VGluT2- axon terminal. We further demonstrated that the segregation between VGluT2-vesicles and VMAT2-vesicles was not altered by *in vivo* overexpression of VMAT2 in mesoaccumbens axons from VGluT2-TH neurons.

Thus segregation between VGluT2-vesicles and VMAT2-vesicles may be conferred by specific retention and sorting signals determined by selective motifs in each of these transporters, as previously documented for other vesicular transporters[20]. Consistent with our ultrastructural findings, both vesicular-immunolabeling and vesicular-immunoprecipitation analysis of purified vesicles from the nAcc indicate lack of VMAT2 and VGluT2 vesicular colocalization. In contrast with our findings, a previous study using enriched membrane preparations from nAcc reported co-immunoprecipitation of VMAT2 and VGluT2[12]. The discrepancy between this earlier work and our findings may be a result of major differences in the material used for immunoprecipitation. We used purified synaptic vesicles instead of enriched membranes. In addition, we used sucrose to avoid organelle disruption, as organelle disruption may result in membrane fusion among different types of membranes. Moreover, we characterized the specificity of the antibodies used for detection of VMAT2, to reduce the likelihood of nonspecific antigen recognition. Together, our ultrastructural findings are consistent with our molecular findings and do not support the previously proposed hypothesis that dopamine and glutamate are packaged and co-released in the nAcc from the same pool of vesicles[1,12,13].

The segregation and retention of glutamate-vesicles and dopamine-vesicles to distinct axonal domains by mesoaccumbens dual VGluT2-TH neurons is in clear contrast with the vesicular organization established by recently discovered dual mesohabenular VGluT2-GABA neurons[21]. Notably, mesohabenular neurons concentrate both glutamate-vesicles and GABA-vesicles in a single axon terminal that establishes excitatory and inhibitory synapses[21]. Thus, VTA VGluT2 neurons are heterogeneous in their molecular composition[6], their ultrastructural properties and signaling mechanisms.

In summary (**Supplementary Fig. 8**), we present converging lines of evidence that the two major classes of identified VTA neurons expressing *Vglut2* mRNA (VGluT2-only and VGluT2-TH neurons[6]) synthesize VGluT2 protein, which accumulates in synaptic vesicles in terminals, forming asymmetric synapses in the nAcc. Consistent with the view that the nAcc asymmetric synapses are excitatory and usually glutamatergic[5], their selective activation evoked excitatory responses in postsynaptic nAcc neurons. We found that mesoaccumbens glutamatergic inputs arising from the VTA could themselves converge on the same postsynaptic target. Our findings also indicate that a single VGluT2 terminal from mesoaccumbens neurons can establish multiple synapses and therefore potentially modulate several neurons in the same brain structure. In addition, we provide direct evidence for dopamine release from mesoaccumbens dual glutamatergic-dopaminergic neurons. Although our findings are consistent with the idea that VGluT2-TH neurons can release both dopamine and glutamate, our results do not support the hypothesis that ATs from these neurons co-release dopamine and glutamate from identical axonal terminals. Rather, our findings indicate that synaptic vesicles that release dopamine or glutamate from mesoaccumbens terminals in both adult rats and adult mice are located in distinct microdomains.

METHODS

Methods and any associated references are available in the online version of the paper.

Note: Any Supplementary Information and Source Data files are available in the online version of the paper.

ACKNOWLEDGMENTS

The viral packaging and *in vitro* testing of the AAV-DIO-VMAT2(Myc) vector were done by the National Institute on Drug Abuse Intramural Research Program Optogenetics and Transgenic Technology Core (OTTC). We thank O. Kiehn and L. Borgius (Karolinska Institutet) for providing the *Vglut2-Cre* transgenic mice and K. Deisseroth (Stanford University) for the *Th-Cre* transgenic rats. Resources for three-dimensional analysis were supported by NS050274. The Intramural Research Program of the National Institute on Drug Abuse supported this work.

AUTHOR CONTRIBUTIONS

M.M. and S.Z. designed the experiments. S.Z., J.Q., X.L., H.-L.W., J.P.B. and A.F.H. performed the experiments. S.Z., J.Q., X.L., H.-L.W., J.P.B., A.F.H., A.B., C.R.L. and M.M. analyzed the data. M.M. wrote the paper with contributions from all of the other authors.

COMPETING FINANCIAL INTERESTS

The authors declare no competing financial interests.

1. Stuber, G.D., Hnasko, T.S., Britt, J.P., Edwards, R.H. & Bonci, A. Dopaminergic terminals in the nucleus accumbens but not the dorsal striatum corelease glutamate. *J. Neurosci.* **30**, 8229–8233 (2010).
2. Tecuapetla, F. *et al.* Glutamatergic signaling by mesolimbic dopamine neurons in the nucleus accumbens. *J. Neurosci.* **30**, 7105–7110 (2010).
3. Bérubé-Carrière, N. *et al.* Ultrastructural characterization of the mesostriatal dopamine innervation in mice, including two mouse lines of conditional VGLUT2 knockout in dopamine neurons. *Eur. J. Neurosci.* **35**, 527–538 (2012).
4. Bérubé-Carrière, N. *et al.* The dual dopamine-glutamate phenotype of growing mesencephalic neurons regresses in mature rat brain. *J. Comp. Neurol.* **517**, 873–891 (2009).
5. Moss, J., Ungless, M.A. & Bolam, J.P. Dopaminergic axons in different divisions of the adult rat striatal complex do not express vesicular glutamate transporters. *Eur. J. Neurosci.* **33**, 1205–1211 (2011).
6. Morales, M. & Root, D.H. Glutamate neurons within the midbrain dopamine regions. *Neuroscience* **282C**, 60–68 (2014).
7. Yamaguchi, T., Wang, H.L., Li, X., Ng, T.H. & Morales, M. Mesocorticolimbic glutamatergic pathway. *J. Neurosci.* **31**, 8476–8490 (2011).
8. Kawano, M. *et al.* Particular subpopulations of midbrain and hypothalamic dopamine neurons express vesicular glutamate transporter 2 in the rat brain. *J. Comp. Neurol.* **498**, 581–592 (2006).
9. Dal Bo, G. *et al.* Dopamine neurons in culture express VGLUT2 explaining their capacity to release glutamate at synapses in addition to dopamine. *J. Neurochem.* **88**, 1398–1405 (2004).
10. Sulzer, D. *et al.* Dopamine neurons make glutamatergic synapses *in vitro*. *J. Neurosci.* **18**, 4588–4602 (1998).
11. Li, X., Qi, J., Yamaguchi, T., Wang, H.L. & Morales, M. Heterogeneous composition of dopamine neurons of the rat A10 region: molecular evidence for diverse signaling properties. *Brain Struct. Funct.* **218**, 1159–1176 (2013).
12. Hnasko, T.S. *et al.* Vesicular glutamate transport promotes dopamine storage and glutamate corelease *in vivo*. *Neuron* **65**, 643–656 (2010).
13. Hnasko, T.S., Hjelmstad, G.O., Fields, H.L. & Edwards, R.H. Ventral tegmental area glutamate neurons: electrophysiological properties and projections. *J. Neurosci.* **32**, 15076–15085 (2012).
14. Descarries, L., Watkins, K.C., Garcia, S., Bosler, O. & Doucet, G. Dual character, asynaptic and synaptic, of the dopamine innervation in adult rat neostriatum: a quantitative autoradiographic and immunocytochemical analysis. *J. Comp. Neurol.* **375**, 167–186 (1996).
15. Yamaguchi, T., Qi, J., Wang, H.L., Zhang, S. & Morales, M. Glutamatergic and dopaminergic neurons in the mouse ventral tegmental area. *Eur. J. Neurosci.* doi:10.1111/ejn.12818 (9 January 2015).
16. Swanson, L.W. The projections of the ventral tegmental area and adjacent regions: a combined fluorescent retrograde tracer and immunofluorescence study in the rat. *Brain Res. Bull.* **9**, 321–353 (1982).
17. Morales, M. & Pickel, V.M. Insights to drug addiction derived from ultrastructural views of the mesocorticolimbic system. *Ann. NY Acad. Sci.* **1248**, 71–88 (2012).
18. Freund, T.F., Powell, J.F. & Smith, A.D. Tyrosine hydroxylase-immunoreactive boutons in synaptic contact with identified striatonigral neurons, with particular reference to dendritic spines. *Neuroscience* **13**, 1189–1215 (1984).
19. Adrover, M.F., Shin, J.H. & Alvarez, V.A. Glutamate and dopamine transmission from midbrain dopamine neurons share similar release properties but are differentially affected by cocaine. *J. Neurosci.* **34**, 3183–3192 (2014).
20. Foss, S.M., Li, H., Santos, M.S., Edwards, R.H. & Voglmaier, S.M. Multiple dileucine-like motifs direct VGLUT1 trafficking. *J. Neurosci.* **33**, 10647–10660 (2013).
21. Root, D.H. *et al.* Single rodent mesohabenular axons release glutamate and GABA. *Nat. Neurosci.* **17**, 1543–1551 (2014).

ONLINE METHODS

Animals and surgical procedures. The anterograde tracer PHA-L (2.5% (wt/vol) in 0.01 M sodium phosphate buffer, pH 7.8; Vector Labs) was applied iontophoretically into the ventral tegmental area (VTA) (bregma AP −5.2, ML ±0.8, DV −8.4) of ten male Sprague-Dawley rats (350–420 g body weight) through a stereotaxically positioned glass micropipette (inner tip diameter of 20 µm, 5-µA current, 5 s on/off for 15 min). Viral vector AAV encoding ChR2 tethered to mCherry under the *Camk2a* promoter (AAV5-CaMKII-ChR2-mCherry, 0.2 µl) was delivered into the VTA by pressure through a glass micropipette attached to a Picospritzer III (Parker Hannifin). Male *Th-Cre* mice (Jackson Laboratory) or *Vglut2-Cre* mice (from O. Kiehn) (background: C57BL/6 J mouse, 25–30 g body weight[22]) were injected into the VTA with Cre-inducible recombinant AAV encoding ChR2 tethered to mCherry (TH-ChR2-mCherry mice or VGluT2-ChR2-mCherry mice). Male *Th-Cre* rats (from K. Deisseroth, 350–420 g body weight[23]) were injected into the VTA with Cre-inducible recombinant AAV encoding VMAT2 inserted with Myc (Myc epitope was inserted in the N terminus of VMAT2; TH-VMAT2(Myc) rats). Rats or mice were anesthetized with isoflurane (Butler Schein) and fixed in a stereotaxic apparatus (David Kopf Instruments for viral injections. The AAV5-DIO-ChR2-mCherry viral vector (AAV-EF1a-DIO-hChR2(H134R)-mCherry-WPRE-pA, 3×10^{12} genomes per ml) from the UNC Vector Core Facility was injected into the VTA of *Th-Cre* mice (0.4 µl) or VTA of *Vglut2-Cre* mice (0.2 µl). The viral vector pAAV-EF1a-DIO-VMAT2(Myc)-WPRE-pA from the Optogenetics and Transgenic Technology Core (NIDA/IRP) was injected into the VTA of *Th-Cre* rats (0.4 µl, 0.1 µl min^{-1}). Each injection was bilaterally with a NanoFil syringe (with 35 gauge needle, WPI) into the VTA (bregma AP −3.4, ML ±0.2, DV −4.3 for mice; bregma AP −5.2, ML ±0.8, DV −8.4 for rats). The micropipette was left in place for an additional 10 min after each injection. The tracer (PHA-L rats, 2 weeks after injection) and viral injected animals (TH-ChR2-mCherry mice, VGluT2-ChR2-mCherry mice and TH-VMAT2(Myc) rats; 6–8 weeks after injections) were used for anatomical, electrophysiological or electrochemical studies. Rats were double housed, and all mice were housed in groups of up to four animals per cage in the animal rooms. Rats and mice were housed in the animal rooms at 22 °C under a 12-h light/dark cycle (light on at 7 a.m.), with *ad libitum* access to food and water.

For anatomical studies, Sprague-Dawley rats without any manipulation, PHA-L rats, TH-ChR2-mCherry mice, VGluT2-ChR2-mCherry mice and TH-VMAT2(Myc) rats were deeply anesthetized with chloral hydrate (35 mg per 100 g), and perfused transcardially with 4% (wt/vol) paraformaldehyde (PFA) with 0.15% (vol/vol) glutaraldehyde and 15% (vol/vol) picric acid in 0.1 M phosphate buffer (PB, pH 7.3). Brains were left in this fixative solution for 2 h at 4 °C, solution was replaced with 2% PFA and left overnight at 4 °C. Brains were rinsed with PB, and cut into coronal serial sections (50 µm thick) with a vibratome (Leica). All animal procedures were approved by the National Institute on Drug Abuse Animal Care and Use Committee.

Immunolabeling for light microscopy. Every fifth section of the VTA or nucleus accumbens (nAcc) was used to detect PHA-L or mCherry by immunohistochemistry. Sections were rinsed with 0.1 M PB (pH 7.3) and incubated with a blocking solution (4% (wt/vol) bovine serum albumin (BSA) in PB supplemented with 0.3% (vol/vol) Triton X-100) for 1 h. Sections were then incubated with either rabbit antibody to PHA-L (AS-2300; Vector Labs, 1:1000 dilution), mouse antibody to mCherry (632543; Clontech Laboratories, 1:500 dilution) or mouse antibody to Myc (05-724; EMD Millipore, Billerica, MA, 1:500 dilution) in the blocking solution overnight at 4 °C. After rinsing in PB, sections were processed with an ABC kit (Vector Labs), and the peroxidase reaction developed with 0.05% (wt/vol) 3, 3-diaminobenzidine-4 HCl (DAB) and 0.003% (vol/vol) hydrogen peroxide (H_2O_2). The specificity of primary antibody to PHA-L or to mCherry was demonstrated by the lack of PHA-L or mCherry immunolabeling in brain sections from rats or mice injected with saline solution without PHA-L, mCherry or Myc.

Pre-embedding immunolabeling. Vibratome brain sections were rinsed with 0.1 M PB (pH 7.3), incubated with 1% (wt/vol) sodium borohydride in PB for 30 min to inactivate free aldehyde groups, rinsed in PB, and then incubated with blocking solution [1% (vol/vol) normal goat serum (NGS), 4% (wt/vol) BSA in PB supplemented with 0.02% (w/v) saponin for 30 min. Sections were then incubated with primary antibodies as follows: rabbit (Rb)-anti-PHA-L; mouse (Ms)-anti-mCherry; Rb-anti-PHA-L + guinea pig (Gp)-anti-VGluT2; Rb-anti-PHA-L + Ms-anti-TH; Ms-anti-mCherry + Gp- anti-VGluT2; Ms-anti-mCherry + Rb-anti-TH; Rb-anti-TH + Gp-anti-VGluT2; goat (Gt)-anti-VMAT2 + Gp-anti-VGluT2; Gp-anti-DAT + Rb-anti-VGluT2, or Ms-anti-Myc + Gp-anti-VGluT2. All primary antibodies were diluted in PB with 1% NGS and incubations were for 24 h at 4 °C, and used at different dilutions: 1:1,000 for Rb-anti-PHA-L, Ms-anti-mCherry, Ms-anti-TH (MAB318; EMD Millipore) and Rb-anti-TH (AB152; EMD Millipore); 1:400 for Gp-anti-VGluT2 (VGluT2-GP-Af240-1; Frontier Institute) and Gp-anti-DAT (DAT-GP-Af720; Frontier Institute); 1:500 for Ms-anti-Myc and 1:250 for Gt-anti-VMAT2 (EB06558). Sections were rinsed and incubated overnight at 4 °C in the corresponding secondary antibodies: biotinylated Gt-anti-Rb (PHA-L single labeling), biotinylated Gt-anti-Ms (mCherry single labeling), anti-Ms-IgG-coupled to 1.4-nm gold (2001; Nanoprobes, 1:100 dilution, Myc detection), biotinylated Gt-anti-Rb (PHA-L detection) + anti-Gp-IgG Fab′ fragment coupled to 1.4-nm gold (2055; 1:100 dilution, VGluT2 detection), biotinylated Gt-anti-Rb (PHA-L detection) + anti-Ms-IgG coupled to 1.4-nm gold (TH detection), biotinylated Gt-anti-Ms (mCherry detection) + anti-Gp-IgG Fab′ fragment coupled to 1.4-nm gold (VGluT2 detection), biotinylated Gt-anti-Ms (mCherry detection) + anti-Rb-IgG coupled to 1.4-nm gold (2003; TH detection; 1:100), biotinylated Gt-anti-Rb (TH detection) + anti-Gp-IgG Fab′ fragment coupled to 1.4-nm gold (VGluT2 detection), biotinylated Gt-anti-Gp (VGluT2 detection) + anti-Rb-IgG coupled to 1.4-nm gold (TH detection), biotinylated Rb-anti-Gt (VMAT2 detection) + anti-Gp-IgG Fab′ fragment coupled to 1.4-nm gold (VGluT2 detection), biotinylated Gt-anti-Gp (VGluT2 detection) + anti-Gt-IgG coupled to 1.4-nm gold (2005; 1:100 dilution, VMAT2 detection), biotinylated Gt-anti-Gp (DAT detection) + anti-Rb-IgG coupled to 1.4-nm gold (VGluT2 detection), or biotinylated Gt-anti-Gp (VGluT2 detection) + anti-Ms-IgG coupled to 1.4-nm gold (Myc detection). Sections were rinsed in PB, and then in double-distilled water, followed by silver enhancement of the gold particles with the Nanoprobe Silver Kit. Next, sections were processed with an ABC kit, fixed with 0.5% (vol/vol) osmium tetroxide, and contrasted in 1% (wt/vol) uranyl acetate. Sections were dehydrated through a series of graded ethanol and with propylene oxide, and flat embedded in Durcupan ACM epoxy resin (EMS). Sections of 70 nm were cut from the outer surface of the tissue with an ultramicrotome UC7 (Leica Microsystems), and collected on formvar-coated grids and counterstained with Reynolds lead citrate.

Post-embedding immunolabeling. Vibratome brain sections from the nAcc shell were rinsed with 0.1 M PB (pH 7.3), incubated with 0.25% (wt/vol) tannic acid in water, rinsed in water, and contrasted in 2% (wt/vol) uranyl acetate (1 h). Sections were dehydrated through a series of graded ethanol, and infiltrated 1:1 volumes of 100% ethanol and 100% LR White (EMS), 1 volume of 100% ethanol: 2 of 100% LR White, and 100% LR White overnight. Resin was polymerized at 60 °C and 70-nm-thick sections were cut and dried overnight, rinsed with PB containing 0.1% (vol/vol) Tween 20 (PB-Tween 20), and incubated with 0.05 M glycine in PB buffer for 15 min. Sections were blocked with 2.5% NGS and 2.5% BSA in PB (1 h), and followed with incubation with Gt-anti-VMAT2 (1:25 dilution). Sections were rinsed and incubated in donkey anti-Gt 12 nm colloidal gold (705-205-147; Jackson ImmunoResearch Laboratories, 1:20 dilution) for 1 h. After rinsed with PB-Tween 20, sections were fixed with 2% glutaraldehyde in PB for 10 min, and then rinsed with PB-Tween 20, and incubated with the blocking solution for 1 h, incubated with Gp-anti-VGluT2 antibody (1:20 dilution) overnight at 4 °C. Sections were rinsed and incubated in anti-Gp 18 nm colloidal gold (706-215-148; Jackson ImmunoResearch Laboratories, 1:10 dilution) for 1 h at 20–25 °C. After rinsed with PB-Tween 20, fixed with 2% glutaraldehyde in PB for 10 min, sections were rinsed with PB-Tween 20, double-distilled water, and counterstained with 5% uranyl acetate and lead.

Sections or vesicles on grids (see below) were examined and photographed using a Tecnai G2 12 transmission electron microscope (FEI) equipped with a digital micrograph 3.4 camera (Gatan). Specificity of primary antibodies has been previous described[24] (see below for anti-VMAT2 antibodies).

Ultrastructural analysis of brain tissue. Serial ultrathin sections of the VTA (bregma −4.92 mm to −6.48 mm) and nAcc (bregma 2.76 mm to 0.96 mm) from 10 male Sprague-Dawley rats and 4 male *Th-Cre* rats were analyzed[25]. We also analyzed serial ultrathin sections of the VTA (bregma −2.92 mm to −3.88 mm) and nAcc (bregma 1.94 mm to 0.86 mm)[26] from 4 male TH-ChR2-mCherry

mice and 4 male VGluT2-ChR2-mCherry mice. Synaptic contacts were classified according to their morphology and immunolabel, and photographed at a magnification of 6,800–13,000×. The morphological criteria used for identification and classification of cellular components observed in these thin sections were as previously described[27]. Type I synapses, here referred as asymmetric synapses, were defined by the presence of contiguous synaptic vesicles in the presynaptic AT and a thick postsynaptic density (PSD) greater than 40 nm (ref. 27). Type II synapses, here referred as symmetric synapses, were defined by the presence of contiguous synaptic vesicles in the presynaptic AT and a thin PSD[27]. Serial sections were obtained to determine the type of synapse. In the serial sections, a terminal containing greater than five immunogold particles were considered as immunopositive terminal. Pictures were adjusted to match contrast and brightness by using Adobe Photoshop (Adobe Systems). This experiment was successfully repeated three times. Electron microscopy and confocal analysis quantification occurred blindly. No statistical methods were used to predetermine sample sizes but our sample sizes are similar to those reported in previous publications[24].

Fluorescence microscopy and image analysis. Coronal brain sections (50 µm) from TH-ChR2-mCherry mice ($n = 4$), VGluT2-ChR2-mCherry mice ($n = 4$) or TH-VMAT2(Myc) rats ($n = 4$) were incubated for 1 h in PB supplemented with 4% BSA and 0.3% Triton X-100. Sections were then incubated with cocktails of primary antibodies: Ms-anti-mCherry (1:500) + Gp-anti-VGluT2 (1:500) + Rb-anti-TH (1:500); Ms-anti-Myc (1:500) + Gt-anti-VMAT2 (1:250) + sheep (Sh)-anti-TH (AB1542; EMD Millipore, 1:500); or Ms-anti-Myc + Gt-anti-VMAT2 + Gp-anti-VGluT2 overnight at 4 °C. After rinsing, sections were incubated with the corresponding cocktails of donkey-fluorescent secondary antibodies (Jackson ImmunoResearch Laboratories, at 1:100 dilution): Alexa-Fluor-488-anti-Gp + Alexa-Fluor-594-anti-Ms + Alexa-Fluor-647-anti-Rb; Alexa-Fluor-488-anti-Gt + Alexa-Fluor-594-anti-Ms + Alexa-Fluor-647-anti-Sh or Alexa-Fluor-488-anti-Gt + Alexa-Fluor-594-anti-Ms + Alexa-Fluor-647-anti-Gp for 2 h at 20–25 °C. After rinsing, sections were mounted with vectashield mounting medium (Vector Labs) on slides. Fluorescent images were collected with Olympus FV1000 Confocal System (Olympus). Images were taken sequentially with different lasers with 100 × oil immersion objectives and Z-stacks were collected at 0.2 µm. Imaris microscopy software (Bitplane) was used to analyze Z-stacks of confocal images from 4 TH-ChR2-mCherry mice or 4 TH-VMAT2(Myc) rats (64 × 64 × 10 µm for each image, 8 images of nAcc from each mouse or rat) to obtain 3-D quantification of ATs expressing mCherry, VGluT2 or TH for mice; Myc, VMAT2, or VGluT2 for rats. The same confocal images were analyzed with the Amira microscopy software (Visualization Sciences Group) to obtain three-dimensional reconstruction of putative synapses. This experiment was successfully repeated three times. No statistical methods were used to predetermine sample sizes but our sample sizes are similar to those reported in previous publications[28]. All statistical analyses were performed with GraphPad prism 5.

Testing of anti-VMAT2 antibodies in western blots from total protein preparations from rat nAcc or from transfected cells expressing VMAT2(Myc). Total protein extracts were obtained from individual slices of the rat nAcc and from transfected cells expressing VMAT2(Myc). For nAcc extracts, 500 µl of 1 × RIPA extraction buffer containing protease inhibitor (Roche Applied Science) was added to nAcc slices. Tissue was homogenized on ice for 30 s, and then centrifuge at 13,200 rpm for 15 min at 4 °C. Supernatant was collected, and protein concentration was measured before stored at −20 °C. For cellular overexpression of VMAT2, we used the plasmid pAAV-EF1a-DIO-VMAT2-WPRE-pA which was constructed previously[29] and obtained from Addgene. To this plasmid, a Myc epitope tag was inserted in-frame with VMAT2 at the N terminus (pAAV-EF1a-DIO-VMAT2(Myc)-WPRE-pA; pOTTC487; see graphic map in **Supplementary Fig. 1**) for immunodetection of transgenic VMAT2. To prepare cell lysates from VMAT2(Myc) overexpressing cells, HEK293 cells were placed in a 24-well plate and transfected the next day using 0.4 µg of pAAV-EF1a-DIO-VMAT2(Myc)-WPRE-pA DNA and 0.4 µg of pAAV-cfos-iCre DNA (pOTTC230) per well, Lipofectamine 2000 transfection reagent (Life technologies) and Opti-MEM reduced serum medium (31985-062; Life technologies). The pOTTC230 plasmid was constructed by the Optogenetics and Transgenic Technology Core (NIDA/IRP; Baltimore, MD). Cells were harvested 2 d after transfection by adding 100 ul of modified RIPA buffer containing 50 mm Tris-HCl (pH 7.4), 0.25% (wt/vol) sodium deoxycholate, 150 mm NaCl, 1 mm EDTA, 1% (vol/vol) Nonidet P-40, and 1 × protease inhibitor mixture (Sigma-Aldrich). The collected samples underwent 3 cycles of rapid freeze-thaw and centrifuged at 12,000 rpm for 10 min at 4 °C. Supernatant from centrifuged cell lysates was collected. Protein concentration was measured and stored at −80 °C until western blot analysis was performed.

Electrophoretic separation of peptides from total protein nAcc extracts and from cell transfected extracts was done by standard electrophoresis. Western blots of nAcc were probed with the following primary antibodies: Gp-VGluT2 (AB2551; EMD Millipore, 1:5,000 dilution); Rb-anti-VMAT2 (ab371945; Abcam); Rb-anti-VMAT2 (Phoenix pharmaceuticals, 1:500); Rb-anti-VMAT2 (ab81855; Abcam, 1:500); Rb-anti-VMAT2 (VMAT2-Rb-Af720; Frontier Institute, 1:1,000); Rb-anti-VMAT2 (138302; Synaptic Systems, 1:1,000); Rb-anti-VMAT2 (AB1598P; EMD Millipore, 1:1,000 dilution); Gt-anti-VMAT2 (SAB2501101; Sigma-Aldrich, 1:1,000), and Gt-anti-VMAT2 (EB06558; Everest Biotech, 1:1,000). Western blots of cell-transfected extracts were probed with the anti-VMAT2 antibody (EB06558) and anti-Myc antibody (1:1,000 dilution) to determine the specificity of the anti-VMAT2 antibody (EB06558). This experiment was successfully repeated three times.

Preparation of synaptic vesicles from nAcc. We tested several experimental conditions to obtain synaptic vesicles, including a previously described method[12], by following this method, we obtained material that under the electron microscope appeared as aggregates of electron-dense material without recognizable ultrastructure. Among the different tested methods, we found that one[30,31] provided in our hands the best yield of synaptic vesicles, which purity was confirmed by electron microscopy. We used 30–40 male Sprague-Dawley rats (6 weeks of age) for each batch of isolation of synaptic vesicles. The isolation of synaptic vesicles was done 3 times from a total of 110 rats. Rats were deeply anesthetized with chloral hydrate (35 mg per 100 g), brains were removed, the nAcc region was dissected out and homogenized in ice-cold 5 mM HEPES buffer (pH 7.4) with 0.32 M sucrose and cocktail of protease inhibitor (Roche Applied Science). For vesicle preparations, materials from 10 rats were processed each time, and all the following steps were performed at 4 °C. The homogenate was then centrifuged at 2,000g for 10 min. The resulting supernatant was centrifuge at 10,000*g* for 30 min. The pellet containing the enriched synaptosomal fraction was homogenized for 5 min after adding 1.6 ml of double distilled water containing protease inhibitors. The osmolarity of this preparation was restored by adding 200 µl of 0.25 M potassium HEPES (pH 6.5) and 200 µl of 1.0 M neutral L-(+)-tartaric acid dipotassium salt buffer (pH 7.5). For immuno-gold labeling and electron microscopy analysis, the supernatant was diluted in HEPES/K^+ tartrate to a final concentration of 0.1 M and processed for immuno-gold EM. For co-immunoprecipitation and western blot experiments, the suspension was centrifuged at 20,000*g* for 20 min, the obtained supernatant was then centrifuged at 55,000*g* for 60 min. $MgSO_4$ buffer (final concentration 1 mM) was added to the supernatant and followed by a final centrifugation at 100,000*g* for 45 min. The pellets containing the isolated synaptic vesicles were resuspended in vesicle assay buffer containing 5 mM HEPES, 0.32 M sucrose, and protease inhibitors. The synaptic vesicles were frozen in liquid nitrogen and stored at −80 °C until use. The purity of the synaptic vesicle preparation was determined under the electron microscope. This experiment was successfully repeated three times.

Ultrastructural evaluation of isolated synaptic vesicles. The purity of the different batches of isolated synaptic vesicles was evaluated following a previously described method with some modification[32]. Pellet harvested in the last step of centrifugation was fixed with 2% OsO_4 for 1 h, briefly rinsed with double-distilled water, and post-fixed with 12% glutaraldehyde in double-distilled water overnight at 4 °C. After fixation, the pellet was rinsed with water and stained with 4% uranyl acetate for 30 min, dehydrated in series of graded ethanol, and embedded with Durcupan ACM epoxy resin. Resin-embedded sections were polymerized at 60 °C for 2 d. Sections of 70 nm were cut with an ultramicrotome UC7 using a diamond knife. The sections were collected on formvar-coated single slot grids and counterstained with Reynolds lead citrate.

Immuno-gold detection of VGluT2 and VMAT2 within the isolated synaptic vesicles. The presence of VGluT2 and VMAT2 within the synaptic membranes of the isolated vesicles was detected following a previously described method with some modification[28]. Synaptic vesicles isolated from the nAcc were diluted

doi:10.1038/nn.3945

with 0.1 M K^+ tartrate/EDTA (1/10, 1/20). 20 µl of isolated vesicles were applied onto formvar and carbon coated nickel grids. Following the formation of a film of solution on the surface of the grid, each grid was immediately placed on top of drops of 4% PFA and fixed overnight at 4 °C. Grids were rinsed with PB, treated with 1 M ethanolamine-HCl for 10 min, rinsed with PB, blocked for 1 h with 10% newborn calf serum (NCS) in 0.1 M Tris/HCl (pH 7.4)/0.3 M NaCl (TBS), and incubated with the first primary antibody (Gt-anti-VMAT2; 1:25 dilution) diluted with 1% NCS/TBS, overnight at 4 °C. After rinsed with 1% NCS/TBS, grids were incubated with the first secondary antibody (donkey anti-goat 12 nm colloidal gold; 705-205-147; 1:20 dilution) in 1% NCS/TBS containing 5 mg/10 ml polyethylene glycol (PEG) for 2 h at 20–25 °C. Grids were rinsed with TBS and fixed with 2.5% glutaraldehyde in PB for 10 min. Grids were rinsed with PB, blocked for 1 h with 1% NCS/TBS, and incubated with the second primary antibody (Gp-anti-VGluT2; 1:20 dilution) diluted with 1% NCS/TBS overnight at 4 °C. After rinsed with 1% NCS in TBS, grids were incubated with the second secondary antibody (donkey anti-Gp-18 nm colloidal; 1:10 dilution) in 1% NCS/TBS/PEG for 2 h at 20–25 °C. Grids were rinsed with TBS and fixed with 2.5% glutaraldehyde in PB for 10 min. After rinsed with double-distilled water, grids were fixed with 1% OsO_4 in PB, rinsed with water, and for negative contrast, grids were rinsed with 3 drops of 1% uranyl acetate and immediately dried on filter paper.

Sections or vesicles on grids were examined and photographed using a Tecnai G2 12 transmission electron microscope (FEI) equipped with a digital micrograph 3.4 camera (Gatan). Specificity of primary antibodies has been previous described[24] (see above for anti-VMAT2 antibodies).

Co-immunoprecipitation and immunoblotting. For co-immunoprecipitation, primary antibodies were cross-linked to protein A or G-coated Dynabeads using the immunoprecipitation kit that includes 'binding and washing buffer' (Life Technologies). Dynabeads were washed in the antibody binding and washing buffer, and incubated with the corresponding primary antibody (Gp-anti-VGluT2 or Gt-anti-VMAT2) with rotation for 10 min at 20–25 °C. After incubation with each primary antibody, beads were washed with the antibody binding and washing buffer. Beads with attached antibody were resuspended with synaptic vesicle solution by adding assay buffer containing 5 mM HEPES, 0.32 M sucrose, and 1× protease inhibitors to obtain a final vesicle concentration of 0.1 µg $µl^{-1}$. Incubation was at 20–25 °C for 100 min with rotation. After incubation, the supernatant was transferred to a clean tube for further analysis. The Dynabeads-Antibody-Vesicles complex was washed four times by using washing buffer and then the sample was gently resuspended in the elution buffer. Proteins from aliquots of the original synaptic vesicle solution, Dynabeads-Antibody-Vesicles elution, and the above supernatant were separated by standard electrophoresis, and western blots of these samples were probed with the following primary antibodies: Ms-anti-VGluT2 (MAB5504; EMD Millipore, 1:2,000), Gt-anti-VMAT2 (EB06558; Everset Biotech, 1:500), and Ms-anti-synaptophysin p38 (MAB638; EMD Millipore, 1:4,000). Western blots immunoprobed for VMAT2 were performed using Quick Western Kit (926-68100; LI-COR). This experiment was successfully repeated three times.

Slice preparation for electrophysiology or voltammetry. 6–8 weeks after virus injection, male VGluT2-ChR2-mCherry mice for electrophysiology and male VGluT2-ChR2-eYFP mice for voltammetry were anesthetized with Euthasol and perfused with ice-cold, artificial cerebrospinal fluid (ACSF), saturated with 95% O_2 and 5% CO_2, and modified to contain (in mM): 92 NMDG, 20 HEPES, 25 glucose, 30 $NaHCO_3$, 1.2 NaH_2PO_4, 2.5 KCl, 5 sodium ascorbate, 3 sodium pyruvate, 2 thiourea, 10 $MgSO_4$, 0.5 $CaCl_2$. Brains were then removed quickly, placed in this same solution on a VT-1200 vibratome (Leica), and sectioned through the nAcc in coronal slices (200 µm thick for electrophysiology or 280 µm thick for voltammetry).

Slice electrophysiology. The slices were placed in a holding chamber filled with the same solution, but held at 32 °C ACSF. For recordings, slices were transferred to a chamber superfused 32 °C ACSF modified to contain (in mM): 125 NaCl, 2.5 KCl, 1.25 NaH_2PO_4, 1 $MgCl_2$, 2.4 $CaCl_2$, 26 $NaHCO_3$ and 11 glucose. Picrotoxin (100 µM) was included in this solution to block inhibitory transmission. Electrodes (3–5 MΩ) were backfilled with an internal solution containing (in mM): 117 cesium methanesulfonate, 20 HEPES, 0.4 EGTA, 2.8 NaCl, 5 TEA-Cl, 3 QX-314, 4 Mg-ATP and 0.4 Na-GTP (280–285 mOsm). Cells were visualized on an upright microscope using infrared differential interference contrast video microscopy. Whole-cell voltage-clamp recordings were made using a MultiClamp 700B amplifier (2 kHz low-pass Bessel filter and 10 kHz digitization) with pClamp 10.3 software (Molecular Devices). Medium spiny neurons in the nAcc shell identified by morphology, membrane resistance, and resting membrane potential, were voltage clamped at −80 mV, unless otherwise noted. Series resistance (10–25 MΩ) was monitored with a 5-mV hyperpolarizing pulse (50 ms) given every 20 s, and only recordings that remained stable over the period of data collection were used. A 200-µm core optical fiber, coupled to a diode-pumped solid state laser, was positioned just above the slice and aimed at the recorded cell. Optically-evoked EPSCs were obtained every 20 s with paired pulses of 473-nm wavelength light (30 mW, 3 ms) using 50-, 100- and 200-ms inter-pulse intervals. AMPA-NMDA receptor response ratios were calculated from EPSCs recorded at both −80 and +40 mV. The AMPAR-mediated portion was obtained by averaging 5 optically evoked EPSCs recorded at −80 mV. The NMDAR-mediated portion was determined by sampling a 5-ms window, 40 ms after the peak AMPAR-mediated current, in EPSCs recorded at +40 mV. Drugs were obtained from either Sigma or Tocris Bioscience. Neurons were randomly and blindly sampled.

Voltammetric measurements of dopamine release in nAcc slices. Before initiating voltammetric recordings, a single brain slice was submerged in a low-volume (170 µl) recording chamber and continuously bathed with warm (30–32 °C) ACSF at 2 ml min^{-1}. The aCSF was warmed using an inline solution heater (TC-324B, Warner Instruments). Fast-scan cyclic voltammetry (FSCV) was performed using carbon fiber electrodes as described previously[33]. Carbon fibers (7 µm diameter, Goodfellow) were aspirated into glass micropipettes, which were then pulled using a vertical electrode puller (Kopf Instuments Model 700-D). Carbon fibers were trimmed to allow ~20–50 µm to protrude from the glass capillary. Pipettes containing the carbon fiber were filled with a solution of 4M K-acetate/150 mM KCl and attached to the head stage of a patch clamp amplifier (HEKA EVA-8, HEKA Instruments). Voltammetric scans, stimulus wave form generation and timing, and data collection were performed using A/D boards (PCI 6052E and PCI-6711E, National Instruments) and custom LabView-based software. All carbon fiber electrodes were tested for stable background currents and responsiveness in ACSF containing dopamine (2 µM) before and following each experiment.

An epifluorescence-equipped upright microscope (Axioskop-2, Zeiss) was used to visualize areas of high YFP expression for recording within each slice. Carbon fibers were placed at a depth of ~75–100 µm within the nAcc. Optical stimulation was delivered to the slice using published methods[34] via an optical fiber (200-µm core, Thorlabs) coupled to a 150-mW, 473-nm diode pumped solid state continuous wave laser system (OEM Laser Systems). The fiber was placed just above the surface of the slice. Optical stimulation consisted of a varying number of 5-ms duration pulses, delivered at 25 Hz. Laser power was kept at <2 mW output in all cases. In some slices, dopamine signals were also elicited by electrical stimulation (5–10 V, 5 × 1-ms pulses, 25 Hz) using a conventional bipolar stimulating electrode consisting of formvar-insulated nichrome wire (50-µm diameter). Voltammetric scans from −0.4 to 1.0 V and back were performed at 400 V s^{-1} (7-ms scan duration) at a frequency of 10 Hz. A 5-s background measurement (50 scans) was taken before stimulation of the brain slice and subtracted from the voltammetric scan obtained at the signal peak immediately after stimulation. This was used to generate a voltammogram (current vs. voltage plot) for each signal. All signals matched those expected for the oxidation and reduction of dopamine. For experiments involving application of glutamate receptor antagonists, signals were taken every 90 s. After obtaining a stable baseline, NBQX (5 µM) and AP-5 (40 µM) were applied to the slice, and the light-evoked dopamine response was monitored over a 10–15-min period. Neurons were randomly and blindly sampled. No statistical methods were used to determine these sample sizes in advance, but sample sizes were based on our previous work using within-slice protocols[21,33,35]. In all cases, we obtained slices from at least two animals to verify the reproducibility of the data set.

Single-cell qRT-PCR of VTA neurons expressing mCherry under the regulation of the *Vglut2* promoter. Male adult VGluT2-ChR2-mCherry mice (n = 3, 25–30 g body weight) were anesthetized with chloral hydrate (35 mg per 100 g body weight), and perfused transcardially with 10% RNAlater (Ambion)

in 0.1 M PB, pH 7.4, as previously described[11]. Brains were immediately removed and frozen in isopentane at −40 °C. Coronal cryosections were used to obtain VTA mCherry labeled neurons for VGluT2 qRT-PCR as previously detailed[36].

Cellular immunodetection of mCherry expressed under the regulation of the *Th* promoter and its coexpression with *Th* mRNA. Male TH-mCherry mice ($n = 3$) were anesthetized with chloral hydrate (35 mg per 100 g) and perfused transcardially with 4% PFA in PB, pH 7.3. The brains were removed, left in 4% PFA for 2 h at 4 °C, and transferred to 18% sucrose solutions in PB overnight at 4 °C. Coronal serial cryosections were processed for dual detection of mCherry immunoreactivity and *Th* mRNA, as previously detailed.

Statistics analysis. Rats and mice in anatomical, electrophysiological and voltammetric studies were excluded from data analysis if the injection sites were incorrect. Image collection and analysis were according to the method of randomization. All statistical analyses applied in anatomy studies were performed with GraphPad Prism 5. In three-dimensional fluorescence microscopy, electron microscopy and voltammetry studies, we performed paired *t* test to analyze data when applicable. Data distribution was assumed to be normal but this was not formally tested. $P < 0.05$ was considered significant.

A **Supplementary Methods Checklist** is available.

22. Borgius, L., Restrepo, C.E., Leao, R.N., Saleh, N. & Kiehn, O. A transgenic mouse line for molecular genetic analysis of excitatory glutamatergic neurons. *Mol. Cell. Neurosci.* **45**, 245–257 (2010).
23. Witten, I.B. *et al.* Recombinase-driver rat lines: tools, techniques, and optogenetic application to dopamine-mediated reinforcement. *Neuron* **72**, 721–733 (2011).
24. Tagliaferro, P. & Morales, M. Synapses between corticotropin-releasing factor-containing axon terminals and dopaminergic neurons in the ventral tegmental area are predominantly glutamatergic. *J. Comp. Neurol.* **506**, 616–626 (2008).
25. Paxinos, G. & Watson, C. *The Rat Brain in Stereotaxic Coordinates* (Elsevier, 2007).
26. Paxinos, G. & Franklin, K.B.J. *The Mouse Brain in Stereotaxic Coordinates* (Academic Press, 2001).
27. Peters, A., Palay, S.L. & Webster, H.d. *The Fine Structure of the Nervous System: Neurons and Their Supporting Cells* (Oxford University Press, 1991).
28. Boulland, J.L. *et al.* Vesicular glutamate and GABA transporters sort to distinct sets of vesicles in a population of presynaptic terminals. *Cereb. Cortex* **19**, 241–248 (2009).
29. Tritsch, N.X., Ding, J.B. & Sabatini, B.L. Dopaminergic neurons inhibit striatal output through non-canonical release of GABA. *Nature* **490**, 262–266 (2012).
30. Erickson, J.D., Masserano, J.M., Barnes, E.M., Ruth, J.A. & Weiner, N. Chloride ion increases [3H]dopamine accumulation by synaptic vesicles purified from rat striatum: inhibition by thiocyanate ion. *Brain Res.* **516**, 155–160 (1990).
31. Teng, L., Crooks, P.A. & Dwoskin, L.P. Lobeline displaces [3H]dihydrotetrabenazine binding and releases [3H]dopamine from rat striatal synaptic vesicles: comparison with d-amphetamine. *J. Neurochem.* **71**, 258–265 (1998).
32. Kadota, K. & Kadota, T. Isolation of coated vesicles, plain synaptic vesicles, and flocculent material from a crude synaptosome fraction of guinea pig whole brain. *J. Cell Biol.* **58**, 135–151 (1973).
33. Good, C.H. *et al.* Impaired nigrostriatal function precedes behavioral deficits in a genetic mitochondrial model of Parkinson's disease. *FASEB J.* **25**, 1333–1344 (2011).
34. Britt, J.P., McDevitt, R.A. & Bonci, A. Use of channelrhodopsin for activation of CNS neurons. *Curr. Protoc. Neurosci.* **2.2**, 16 (2012).
35. Qi, J. *et al.* A glutamatergic reward input from the dorsal raphe to ventral tegmental area dopamine neurons. *Nat. Commun.* **5**, 5390 (2014).
36. Root, D.H., Mejias-Aponte, C.A., Qi, J. & Morales, M. Role of glutamatergic projections from ventral tegmental area to lateral habenula in aversive conditioning. *J. Neurosci.* **34**, 13906–13910 (2014).

doi:10.1038/nn.3945